PREPRINT UCRL- 83316

Lawrence Livermore Laboratory

A Numerical Study of Laminar Wall Quenching

Charles K. Westbrook, A. A. Adamczyk and G. A. Lavoie

August 1979

This paper was prepared for submission to The Combustion Institute Western States Section meeting, October 15-16, 1979, Berkeley, California.

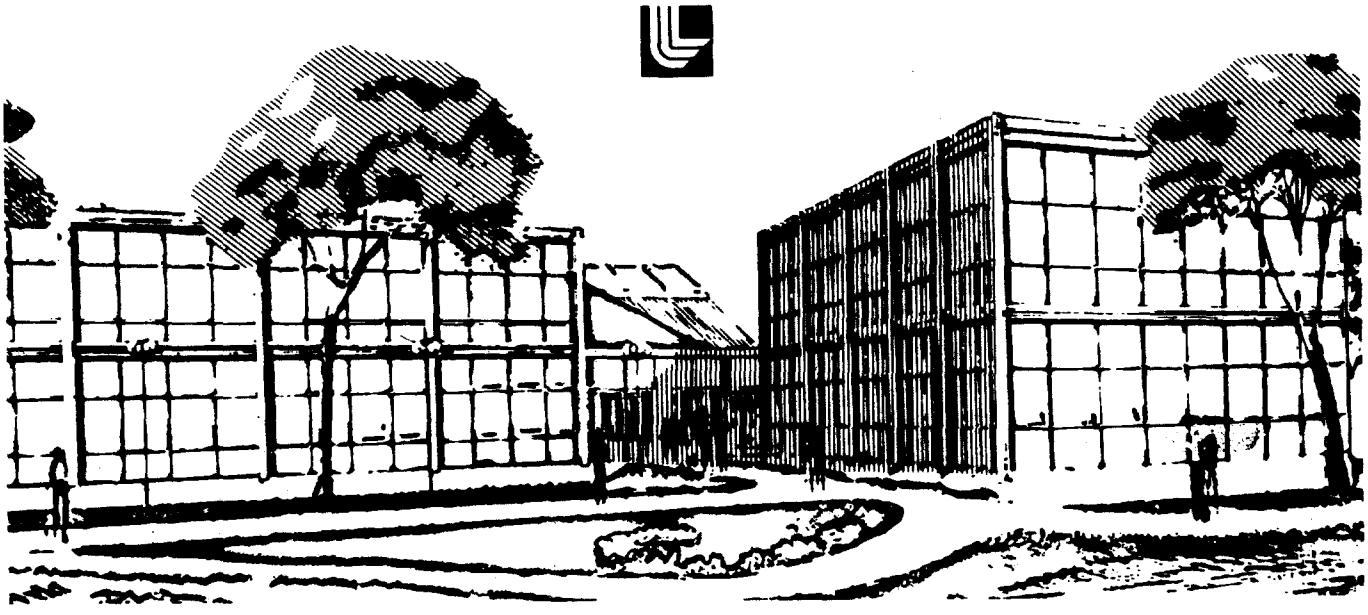

A Numerical Study of Laminar Wall Quenching

Charles K. Westbrook

Lawrence Livermore Laboratory, University of California

Livermore, California 94550

A. A. Adamczyk and G. A. Lavoie

Ford Motor Company

Dearborn, Michigan 48121

ABSTRACT

Laminar flame quenching at the cold wall of a combustion chamber has been studied, using a numerical model to describe the reactive flow. The model combines an unsteady treatment of the fluid mechanics and a detailed chemical kinetic reaction mechanism. Fuels considered included both methane and methanol. The one-dimensional case of flame propagation perpendicular to the wall was studied. Two reference cases are described in detail for flame quenching at 10 atmospheres pressure and a wall temperature of 300 K with stoichiometric mixtures of methane-air and methanol-air. In each case a conventional laminar flame propagates toward the wall, approaching to within a distance determined by the thermal flame thickness. Chemical kinetic factors, particularly differences between the temperature dependence of radical recombination reactions and conventional chain branching and chain propagation reactions, are shown to be responsible for quenching the flame near the wall. The flame stagnates, but fuel remaining near the wall diffuses out of the boundary region

and is rapidly oxidized away from the wall. Subsequent model calculations demonstrate the effects of variations in pressure, fuel-air equivalence ratio, wall temperature, and type of fuel. Computed results from these methane and methanol flame quenching models indicate that the total unburned hydrocarbon content is considerably smaller than is commonly believed and that thermal wall quenching may not be the major source for hydrocarbon emissions from internal combustion engines at near-stoichiometric conditions.

INTRODUCTION

Knowledge of the chemical and fluid mechanical processes which control exhaust emissions from internal combustion engines is of great importance in developing new fuel-efficient engines while satisfying emission constraints. In particular, it would be extremely useful to have, as an aid in design, a comprehensive computer model to simulate engine efficiency and emissions. Currently, performance characteristics, NO_x and CO emissions can be modeled with reasonable accuracy for the conventional homogeneous-charge engine [1]. However, models of hydrocarbon emissions have been slow to develop, largely because the fundamental factors controlling HC emissions are still poorly understood [2].

Hydrocarbons in internal combustion engine exhaust can arise from a variety of sources within the engine. A number of workers have identified flame wall quenching, crevice volumes and surface deposits [3-5] as possible sources for HC emissions. Based on engine photography and sampling valve measurements, Daniel [3,6] identified the flame wall interaction process, near

the relatively cold combustion chamber walls, as an important contributor to hydrocarbon emissions. Furthermore, Agnew [7], in conducting combustion bomb experiments, also concluded that the wall quenching process was the major source of residual hydrocarbons from this type of single-shot device. Based on these experiments, it was felt at the onset of this study that the wall quenching problem warranted further attention, and in particular that useful insight could be gained by detailed numerical modeling of the quench layer.

Mathematically, two distinct wall quenching configurations can be identified. Side-on quenching occurs when the flame propagates along a cold surface with only a single contact point between the flame and the cold wall, while head-on wall quenching refers to the situation in which a propagating flame encounters a cold obstacle in its path. Side-on quenching has been described in terms of a two-dimensional boundary layer problem by von Karman and Millan [8] and Fendell [9], while head-on flame quenching has been modeled as a one-dimensional, non-steady process by Kurkov and Mirsky [10], Adamczyk and Lavoie [11] and Carrier et al. [12]. In these descriptions of quenching processes, either a simple heat release schedule or one-step chemical kinetics was used to describe the characteristics of the propagating flame structure. One significant aspect of these head-on quenching models is that they were unable to account for the high levels of hydrocarbons observed in the engine experiments of Daniel [6], or Agnew's combustion bomb experiments [7]. The suggestion was made by Adamczyk and Lavoie [11] that improved agreement might be obtained with the use of detailed chemical kinetics in these models

Accordingly, in the present study an extended detailed chemical kinetics treatment is employed, together with the equations of laminar unsteady fluid

mechanics, to model the head-on flame quenching process. The study includes an analysis of the detailed flame structure during quenching and post-quenching oxidation for methane and methanol flames for a variety of pressure levels, equivalence ratios and wall temperatures.

NUMERICAL MODEL

The mathematical formulation of the equations describing the evolution of a laminar flame in a one-dimensional planar geometry has been discussed by Lund [13]. This model has been used in a variety of studies of laminar flame propagation [14,15] and has been found to predict flame speed and flame thicknesses which agree well with experimental results over a wide range of conditions for both methane and methanol fuels. The conservation equations for mass, momentum, and energy, together with the definitions of the species and energy flux terms and the equation of state are summarized in Table I. Conventional notation is used unless otherwise indicated. Detailed definitions can be found in reference [13].

Finite difference equations are formulated for the governing equations, including the chemical kinetic terms from the reaction mechanism. These difference equations are solved implicitly in time in order to account for the stiffness of some of the chemical kinetic terms. The kinetic equations, hydrodynamic equations, and energy equation are all solved simultaneously using a block tridiagonal matrix inversion method described in reference [13]. This method permits a larger time step and exhibits better convergence and stability characteristics than most conventional operator-splitting techniques. The numerical model also uses a variable and non-uniform spatial grid

algorithm which concentrates spatial nodes in the region of large temperature gradient, a feature which is essential if these calculations are to be carried out efficiently. One important term has been added to the energy conservation equation to account for heat transfer from the reacting gas medium to the wall of the combustion chamber. We assume for simplicity that the chamber wall remains at a fixed temperature T_w. The spatial zone in the chamber nearest to the wall is forced to remain at the same temperature as the wall by including a heat sink term S_w in the energy equation, with

$$S_w = S_0 (T_w - T) \quad .$$

S_0 is set large enough to keep the temperature in the last zone equal to T_w. This treatment of wall heat transfer is equivalent to assuming that the wall has an infinite heat capacity. In practice the wall temperature is known to vary only about 10 K during quenching [16], so the approximation used here should be an adequate characterization of the processes occurring.

CHEMICAL KINETICS

The detailed chemical kinetic reaction mechanism was taken directly from Westbrook and Dryer [17] and used without modification for these calculations. This mechanism, given in Table II, reproduces experimental data for shock tube ignition and oxidation of methane [18], turbulent flow reactor methane oxidation [19], and shock tube and flow reactor oxidation of methanol [17]. In addition, the reaction mechanism, combined with the fluid mechanical treatment described in the previous section, accurately

reproduces laminar flame speed data for both methane and methanol over wide ranges of pressure, unburned gas temperature, and equivalence ratio [14,15], requiring only a single adjustment of the transport coefficients as described in reference [17]. As a result, the reaction mechanism represents a well-validated chemical kinetic model which can be used to predict laminar flame behavior under a wide variety of conditions.

One of the serious theoretical problems in earlier analytical quench zone models (e.g. references [20,21]) has been the characterization of the laminar flame speed, including its dependence on pressure, equivalence ratio, and initial conditions. In most of these models the flame speed was assumed to vary as P^{α}, where α is determined experimentally. In addition the temperature dependence of the flame speed was assumed to be proportional to a single Arrhenius term with an apparent activation energy E. Applications of the detailed kinetic modeling approach have shown [15] that the pressure exponent α depends on the unburned gas temperature and on density and varies from one fuel to another. In particular, values determined for α in flame studies near atmospheric pressure are not correct at elevated pressures (i.e. above 5 atm [15,22]). The use of a single apparent activation energy E ignores the fact that, due to the different temperature dependence of each elementary reaction, different mechanistic steps are responsible for fuel oxidation in different temperature and pressure regimes. Other approximations are required in the simplified kinetics models to account for the effects of variations in equivalence ratio and wall temperature. The reaction system given in Table II eliminates the need to make these approximations and is able to describe in fundamental terms the mechanisms of flame propagation and flame extinction over a wide range of operating conditions.

Another distinct advantage of a detailed kinetics model lies in its ability to predict the relative amounts of chemical intermediate species which are formed during the quenching process. In the case of alcohol fuels the aldehyde emissions are particularly important, and since acetylene is widely considered to be a major soot precursor, C_2H_2 levels in both methane-air and methanol-air flames are also of interest.

Most of the elementary chemical reactions and rates in Table II have been developed primarily to describe fuel oxidation at intermediate and high temperatures, above 800 K. Oxidation rates for temperatures around 300 K are so low that they can be neglected in flame environments. However, one of the interesting features of wall quench phenomena is the importance of radical recombination reactions in the cold boundary layer. The rates of these recombination reactions in Table II are uncertain at low temperatures. As a result, the actual concentrations of species formed by these reactions must be considered as approximate values. However, predicted trends in the production rates of these species with changes in operating conditions should be reliable and provide a good indication of the major chemical features of flame quenching.

FLAME QUENCHING MODELS

The geometry under consideration for laminar head-on flame quenching consists of a planar region one centimeter in thickness. One boundary consists of a rigid wall held at a fixed temperature T_w, and the other boundary is open. The gas velocity normal to the wall must go to zero at the rigid wall, while gas is free to flow in either direction through the open boundary. The boundary condition used at the open boundary of the chamber

is represented as a prescribed gas pressure, combined with a zero spatial derivative for temperature and species mole fractions. Thus material flows in or out of the open boundary in response to the pressure gradient. However, since flames propagate at speeds much less than sonic velocity, the process is essentially isobaric. Therefore these calculations represent wall quenching at constant pressure.

For each calculation a flame was established at a distance from the cold wall. In each case the full kinetics scheme and 40 spatial zones were used. The flame region itself contained 8-10 zones, and the variable grid algorithm continuously adjusted the spatial zoning to follow the flame. The flame then began to propagate across the remainder of the combustion chamber towards the cold wall. The general features of the wall quenching geometry are summarized in Figure 1.

Flame model calculations were carried out over a wide range of conditions to determine quenching behavior. Initial pressure levels were varied in a range from 1-40 atmospheres, wall temperatures of 300 K and 400 K were included; fuel-air equivalence ratios were specified between 0.8 and 1.4; and both methane and methanol were used as fuels. For each calculation, the unburned gas was initially at rest at the temperature of the wall. The flame was located initially far enough from the wall that it was not affected by the presence of the wall and was free to travel several flame widths before the influence of the wall was felt. This condition could be verified by plotting the flame speed as a function of time, being careful that the flame propagated at a constant speed for some time. Once the influence of the wall begins to be felt the flame speed will change and eventually go to zero as the flame stagnates in the boundary layer as described below.

Several definitions of flame width and position have been used to describe the computed results. The most relevant measure of flame thickness was found to be the thermal width L_t , defined graphically in terms of the maximum temperature gradient in the flame zone. At the point of maximum temperature gradient a straight line is drawn with a slope equal to that maximum gradient. The locations at which this line intercepts the adiabatic flame temperature and the unburned gas temperature T_u define the flame width. This procedure is illustrated in Figure 1. Two possible definitions of flame position were used in this study. In the first method, the point x_t in the flame at which the gas temperature is some convenient value (1500 K for these flames) is defined as the flame position. For the second definition, x_r is the position in the flame where the maximum rate of heat release due to chemical reactions occurs. In most cases studied x_r corresponds to a gas temperature slightly higher than 1500 K. For steady flames without walls, both x_r and x_t give the same results for flame velocity even if they do not correspond to exactly the same location in the flame. As the flame approaches a cold wall and stagnates, the minimum position of either x_r or x_t can be used as a reasonable definition of the quench distance q. In the calculations described here, x_t has been used primarily. With these definitions established, the reference model will be discussed in detail, followed by a description of the effects of variations in operating parameters.

REFERENCE MODEL - METHANOL

In order to illustrate the principal features of these flame quenching calculations, one case was selected to be described in detail. For this case, the fuel is a stoichiometric methanol-air mixture at 10 atmospheres pressure. This pressure was chosen because it is close to the pressure at the time of quenching in a constant volume combustion bomb initially at atmospheric pressure. The wall temperature is 300 K, and the initial unburned fuel is 12.3% of the total mixture.

Before the flame begins to encounter the wall, the flame speed (29 cm/sec) and the species and temperature profiles through the flame are identical with those determined for the same conditions without the wall [15]. Some of these profiles are presented in Figure 2, including the temperature, major species, and some of the major radical and stable intermediate species. Of particular interest in this application is the induction region just in front of the flame. In this region, extending about 0.1 mm ahead of the flame, radical species which have diffused out of the flame zone react with fuel and other intermediate species. The most important reactions for CH_3OH consumption are

$$CH_3OH + OH = CH_2OH + H_2O \qquad (3)$$

$$CH_3OH + H = CH_2OH + H_2 \qquad (5)$$

with other key reaction including

$$CH_2OH + O_2 = CH_2O + HO_2 \qquad (10)$$

$$CH_2O + OH = HCO + H_2O \qquad (26)$$

$$HCO + M = H + CO + M \qquad (31)$$

$$HCO + O_2 = CO + HO_2 \qquad (35)$$

These reactions perform the preliminary decomposition of the fuel molecule, breaking it apart into smaller molecules and radical species which can easily

be oxidized in the flame zone itself. This situation prevails until the induction region approaches the colder wall region.

To understand the next phase of this problem, it is necessary to examine the reaction mechanism of Table II. The activation energies of the above reactions between radicals and fuel molecules are 2 kcal/mol or greater. For temperatures above about 800 K the rates of these reactions are high enough that they represent the major path by which these radical species are consumed. However, radical recombination reactions provide an alternative path for radical consumption. These reactions typically have very small activation energies. The activation energies for Reaction 54 and the reverse reactions for Reactions 1, 11, 25, 31, 46, 52, 55, 56, and 57 are all less than 2 kcal/mol. When the temperature in the induction region falls below 700-800 K then the rates of the radical-fuel reactions fall to very low values; radical recombinations, with small activation energies then become the dominant means of consumption of radical species. Similar quenching mechanisms have been observed in modeling studies of rapidly expanding combustion chambers [23], of stratified charge combustion [24,25], and of pressure inhibition of laminar flames [17]. The most important of the recombination reactions in these models are

$$H + O_2 + M = HO_2 + M \qquad (46)$$

$$CH_3 + OH + M = CH_3OH + M \qquad (1)$$

$$CH_3 + CH_3 = C_2H_6 \qquad (57)$$

$$CO + O + M = CO_2 + M \qquad (38)$$

In the methane flames Reaction 11 is also significant.

$$CH_3 + H + M = CH_4 + M \qquad (11)$$

As the flame approaches the cold boundary, radical recombination reactions remove so many radical species that not enough radicals remain to consume any fuel, so the flame halts. Temperature and species concentration profiles at the time of quench t_q, when the flame no longer propagates toward the cold wall, are summarized in Figure 3. Several features are immediately evident. First, most of the remaining unburned hydrocarbons consist of the original fuel. The CH_2O level is less than 5% of the CH_3OH value, with the CH_4 and others even lower. The fuel and stable intermediate species (CH_3OH, H_2, CH_4, CH_2O, H_2O_2, C_2H_6, C_2H_2) have their peak values at or near the wall, while the radical species (H, O, OH, HCO, CH_3, HO_2, CH_2OH) reach their peak values some distance from the wall. This spatial arrangement is in contrast with the case shown in Figure 2 for the unquenched flame, in which the peak values for nearly all of these species lie close together in the flame region. The cold wall has drastically changed the flame structure by inhibiting all of the reactions with activation energies greater than 1-2 kcal/mol. Since this includes both pyrolysis and chain branching reactions, only radical recombination reactions can proceed. The region near the wall, which would have been the flame zone, is depleted of radicals. Since reactions with radicals are the primary means of consuming the stable intermediate species, this means that there is no effective way to consume these species in the wall region. The radical species have their peak values at a distance from the wall, where the local gas temperature is in the range 1500-1800 K, and where chain branching reactions can maintain high radical species concentrations.

The ensuing phase in the evolution of the wall-flame system is controlled by the rate at which fuel and stable intermediate species can diffuse away from the wall region into the much higher temperature region where radical species

concentrations are high. In this reaction zone, the fuel-radical reactions can proceed rapidly, consuming the remaining fuel. The important parameter here is the characteristic time for this diffusion-limited fuel oxidation. In Figure 4 we show the fuel mole fraction profiles at a sequence of times subsequent to t_q. At t_q the methanol mole fraction near the wall is close to 5%, but 0.347 ms later it has dropped to 0.25%. At a still later time, 2 ms after quench (not shown) the fuel concentration at the wall is less than 30 ppm. Thus, in this case, there is a significant amount of residual fuel consumption over a time scale of 2 milliseconds or less.

During this diffusion-limited fuel oxidation period, heat losses to the wall are greater than the rate of energy release from chemical reactions. As a result, the reaction zone moves slowly away from the wall. Using x_t as the definition of flame position, we plot the flame position as a function of time in Figure 5. The minimum value of x_t conveniently defines the quench distance q_t and the quench time t_q. The quench distance q_t is approximately 0.064 mm for the methanol-air reference model. Also shown in Figure 5 is the unburned fuel concentration, expressed in parts per million and averaged over the calculation volume. In all model results to be described, the fuel comprised 90% or more of the unburned hydrocarbons at any given time, so in these discussions we will generally present only fuel concentrations. The calculation volume has a depth of one centimeter, and the surface-to-volume ratio of this configuration is equal to unity. Therefore the calculated average concentrations can be used to approximate values for other geometrical configurations by multiplying by the actual surface-to-volume ratio (cm^{-1}) in the case of constant pressure combustion, and by $\gamma = C_p/C_v$ and the surface-to-volume ratio for constant volume combustion.

REFERENCE MODEL - METHANE

The reference model calculation was repeated, with methane replacing the methanol as fuel. The pressure remained at 10 atm and the wall temperature at 300 K. Again the flame begins to propagate towards the wall, but at a velocity of only 14 cm/sec, consistent with values reported by Andrews and Bradley [26] for methane-air under these conditions. All of the general features of the methanol flame quenching are repeated for the methane flame, but with time and space scales which are larger than for methanol. The thermal quench distance q_t is about 0.12 mm, twice the value found in the methanol model. Using the quench time as the reference point for the two models, the average unburned fuel concentrations for both methanol and methane are shown in Figure 6. The steeper slope of the methanol curve for times less than t_q reflects the larger flame speed in the methanol model. The lower amount of fuel remaining at t_q in the case of methanol is a result of the fact that the methanol flame has a considerably smaller flame thickness. Therefore the methanol flame is able to get closer to the wall before feeling the effects of the cold boundary. A larger fraction of the fuel near the wall is thus consumed prior to quenching with methanol as the fuel. This closer approach has another very significant effect on the subsequent oxidation of fuel in the diffusion-limited phase of the evolution. Because the hot flame zone is closer to the wall for methanol, the fuel remaining in the quench layer has a much smaller distance over which to diffuse and is oxidized much more rapidly. This more than compensates for the fact that CH_3OH, with its higher molecular weight relative to CH_4, will have a correspondingly lower diffusion velocity.

The results are consistent with the idea that the quench distance and the amount of unburned fuel at the time of quenching can be correlated directly with the flame thickness. Since the flame thickness correlates approximately inversely with the flame speed (Semenov [27]), this should result in a relation between quench distance, unburned fuel, and flame speed. In the 10 atm reference models, the flame speeds are 14 cm/sec and 29 cm/sec, the quench distances are 0.12 and 0.064 mm, and the unburned fuel concentrations at t_q are 1600 ppm and 700 ppm, all consistent with this type of correlation. In more general terms, one would expect a correlation to exist such that the non-dimensional burned gas Peclet number is approximately constant [28], i.e.

$$Pe_b = \rho_u S_u q_t C_{p_b}/k_b \cong \text{constant}$$

where ρ_u is the unburned gas density, S_u is the flame speed and C_{p_b} and k_b are the specific heat and thermal conductivity of the gas evaluated at the burned gas conditions (adiabatic flame temperature). As will be seen, the results were found to be in good agreement with this relationship.

EFFECTS OF EQUIVALENCE RATIO

With the pressure remaining at 10 atm, further model calculations were carried out to assess the effects of variations in fuel-air equivalence ratio on quench parameters. For both fuels, quench studies at ϕ = 0.8, 1.0, 1.2, and 1.4 were carried out. The qualitative features of the flame propagation, stagnation, and diffusion-limited fuel oxidation were again similar to the reference models. The quench distances for these models are plotted in

Figure 7, in which curves have been drawn connecting the computed points. These curves closely resemble the reciprocals of curves for flame speed for methane [26] and methanol [15] as functions of equivalence ratio at constant pressure, including the indication that methane has its maximum flame speed at an equivalence ratio closer to stoichiometric than does methanol. Using flame speed results for methanol from reference [15] it was found, for values of equivalence ratio $0.8 \leq \phi \leq 1.4$, that the burnt gas Peclet number is equal to $1.0 \pm .2$. This result is in good agreement with the single-step reaction model of Adamczyk and Lavoie [11], and similar to the values of other simple models [20,21].

The chemical composition of the quench zone depends strongly on overall equivalence ratio. In the stoichiometric reference model for methanol, the amounts of CH_4, C_2H_6, C_2H_4, and C_2H_2 in the quench layer are very small. Methane reaches 100 ppm near the wall but falls off rapidly with distance from the wall, and the C_2 species are lower than methane by a factor of ten. However, in the $\phi = 1.4$ case, the methane levels are higher than in the stoichiometric case by a factor of nearly 50, exceeding 1000 ppm near the wall at the time of quenching. The C_2 species also increase proportionally. At the time of quenching, the average and peak concentrations in the calculation for $\phi = 1.4$ are C_2H_2 (20 ppm, 400 ppm), C_2H_4 (6 ppm, 200 ppm), C_2H_6 (4 ppm, 120 ppm) and CH_4 (45 ppm, 1200 ppm). These species are oxidized in the flame zone, which lies a distance of approximately q_t away from the wall, over a time scale controlled by diffusion of these species and the fuel away from the wall region. Even in the richest cases studied, the original fuel accounts for at least 90% of the hydrocarbons

in the quench layer at all times. The relative abundance of CO and CO_2 also depends strongly on equivalence ratio, as does the abundance of H_2. Both CO and H_2 are present in much larger amounts in the rich cases than in the lean and stoichiometric cases.

For the methane flames, compositional variations with equivalence ratio are similar to those for methanol. The relative abundances of the C_2 species in the methane quench zone rise rapidly with increasing equivalence ratio. There is a pronounced shift towards C_2H_2 as equivalence ratio increases; at $\phi = 1$, the ratio $C_2H_2(avg)/C_2H_6(avg) = 1/2$, while the same ratio at $\phi = 1.4$ is nearly 7. In the richest methane case the peak local acetylene concentration near the cold wall is about 3500 ppm. Methanol seems to be formed in the quenched methane flames through the recombination of methyl and hydroxyl radicals,

$$CH_3 + OH + M = CH_3OH + M \qquad (1)$$

achieving concentrations near the wall at t_q of the order of 100 ppm. The methanol formed in this manner is then oxidized during the diffusion-limited phase of the fuel consumption.

The remaining unburned fuel for both methane and methanol fuels is plotted in Figure 8, showing the dependence on equivalence ratio. Again the differences in laminar flame speed are responsible for the different slopes for times prior to t_q. It is worth noting that all but one of the curves fall well below 1000 ppm within 0.5 ms after t_q. The exception is the richest ($\phi = 1.4$) methane flame, which has a considerably slower fuel consumption rate than all the other cases.

EFFECTS OF PRESSURE

A series of calculations was carried out using both fuels in stoichiometric mixtures at pressures of 1, 10, and 40 atmospheres. Quench distances are expressed in terms of pressure for all cases in Figure 9. The predicted results are in good agreement with the experimental single wall quench distances of Daniel [3], and Ellenberger and Bowlus [32], obtained for stoichiometric propane-air mixtures. The calculated curves show a steady decrease in quench distance with increasing pressure. Since flame thickness also decreases with increasing pressure, this trend represents a correlation between flame thickness and quench distance. Both curves in Figure 9 are nearly straight lines on this log-log plot, with slightly more curvature in the results for the methane flames. If we use the quench distances at 1 and 40 atm to define a straight line for each fuel, we get

$$q_t = 0.5\ P^{-0.56} \qquad CH_4$$

$$q_t = 0.48\ P^{-0.88} \qquad CH_3OH$$

Using high pressure flame speed correlations for methane [22,26] and for methanol [15] as functions of pressure, we find

$$S_u \times q_t \sim 43\ P^{-0.5} \times 0.5\ P^{-0.56} = 2.1\ P^{-1.06} \qquad CH_4$$

$$S_u \times q_t \sim 44\ P^{-0.18} \times 0.48\ P^{-0.88} = 2.1\ P^{-106} \qquad CH_3OH$$

or in terms of the Peclet number,

$$Pe_b = 1.0\ P^{-0.06}$$

for both fuels. Since both the flame speed and quench distance values are

subject to uncertainties as large as ± 10%, the agreement between the correlations for the two fuels is somewhat fortuitous. However, it appears reasonable to suggest that a correlation of the form

$$S_u \times q_t \simeq 2\ P^{-1} \qquad \text{or} \qquad Pe_b \simeq 1.0$$

For both fuels would accurately describe the computed quench distances. Quenching at pressures below atmospheric was not included in this study, but it has been shown [15] that the flame speed-pressure correlation changes somewhat for both fuels in this regime due to the decreasing influence of radical recombination reactions, so the above quench distance-flame speed correlation with pressure may not be valid at pressures substantially below atmospheric.

The fuel remaining unburned as a function of time relative to the flame stagnation time in each model is shown in Figure 10. At t_q the atmospheric pressure flames for CH_4 and CH_3OH show about the same amounts of residual fuel, while at elevated pressures and equal times after t_q the methanol flames have smaller unburned fuel concentrations than the methane flames.

For methanol the largest decrease in fuel concentration at t_q is between 1 and 10 atm pressure, with a smaller decrease to 40 atm. These results are summarized in Figure 11. The subsequent evolution of each model during the diffusion-limited fuel oxidation phase tends to maintain the shapes of the curves in Figure 11. Diffusion of fuel is more rapid as the pressure increases because the higher pressure flames stagnate closer to the wall, so the fuel has a considerably shorter distance to diffuse to encounter the higher temperature oxidation region.

EFFECT OF TEMPERATURE

One further calculation was carried out to assess the effects of variation in the unburned gas and wall temperature. These temperatures were set to 400 K, with the pressure at 10 atm. The fuel was a stoichiometric methanol-air mixture. Qualitatively the quenching of this flame was similar to those described earlier. Fuel remaining as a function of time, relative to t_q, is plotted in Figure 12, together with the results for the methanol-air reference model. The higher temperature flame has a higher initial velocity, due to the dependence of the laminar flame speed on temperature. Less fuel remains at t_q in the higher temperature case, primarily because the flame is thinner and therefore stagnates closer to the wall. Diffusion in this case is rapid, since the flame comes closer to the wall and the laminar transport coefficients increase with local gas temperature.

DISCUSSION

The quantities of interest in quenching phenomena are the single-wall quench distance and the amount of remaining fuel in the combustion chamber, quantities which are very difficult to determine experimentally. These calculations have shown that these quench parameters can be correlated with flame properties such as the laminar flame speed which are much easier to obtain, including the effects of variations in equivalence ratio and pressure for both methane and methanol flames. It would be very useful to find that these computed results could be used to predict quench phenomena for additional fuels. Flame speed data are well known for many practical fuel-air mixtures. An interesting example of such a fuel is propane, for which a detailed chemical kinetic mechanism has not yet been developed or validated. However, Metghalchi and Keck [29] have determined laminar flame speed data for stoichiometric propane-air mixtures as a function of pressure, using a constant volume combustion bomb. They found that the flame speed was proportional to $P^{-0.17}$, a pressure exponent close to the value of -0.18 found [15] for methanol-air mixtures. If the correlations derived earlier for quench distance and unburned fuel for methanol can be applied to propane-air mixtures, one could then estimate the quench distance and residual hydrocarbon material for this fuel. Because of the unusually large dependence of laminar flame speed on pressure for methane, methane behaves in a somewhat different way. The oxidation of methane is kinetically anomalous in a sense because of its dependence on methyl radical recombination [19], so one might expect computed results for methanol to be more typical of hydrocarbon fuels other than methane.

Direct comparison of these results with experiment is difficult because of the lack of experimental data. In general, however, the predicted quench distances are similar to the few measured values of single-wall quench distance that are available [3,32], (see Figure 9), and follow the trends of two plate quench data [28].

Regarding the residual fuel content in the layer, we note from Figures 8 and 10 that a typical time constant for the diffusion-limited residual fuel oxidation is on the order of one millisecond for near-stoichiometric mixtures. For conventional engines, operating at normal conditions, there is ample time (3-30 ms) to accomplish this diffusive fuel consumption. With typical surface-to-volume ratios of $\sim 2\ cm^{-1}$, and for near-stoichiometric conditions, these results indicate that the laminar flame quenching process produces on the order of 10-30 ppm 'C' of unburned hydrocarbons, a level which is considerably lower than measured exhaust levels of 500-100 ppm 'C'. Further, these results are in general agreement with the recent sampling valve experiments of LoRusso et al. [31] who found significant post-quench oxidation occurring within 1 ms of flame quenching in an engine operated at an equivalence ratio of 0.9.

It is also interesting to note that since this work was begun, new results from combustion bomb experiments have become available [30], which show overall HC levels more than an order of magnitude below those previously reported in the literature [7]. These low levels were achieved by carefully reducing crevice volumes in the bomb. It is not clear at this time whether the values reported represent a lower limit to surface-generated hydrocarbons or if the emissions are due to additional unaccounted-for crevices. In any case, the levels ($\sim$ 100 ppm 'C' for $S/V = 0.8\ cm^{-1}$) are significantly lower

than engine measurements, which would involve larger crevice volumes, tending to support the quenching mechanism proposed here.

This study is limited to the one-dimensional case of head-on quenching and assumes that there is a laminar flow region near the combustion chamber wall. Other mechanisms which may be responsible for hydrocarbon emissions have not been addressed. This study has attempted to characterize one possible source of pollutant emissions and has indicated that this process does not produce sufficient quantities of hydrocarbons to explain the emissions from homogeneous-charge engines under normal operating conditions.

ACKNOWLEDGEMENTS

We wish to express our gratitude to Dr. Frederick L. Dryer of Princeton University and to Julian A. LoRusso of Ford Motor Company for many fruitful discussions of this subject, and to Lila L. Chase of Lawrence Livermore Laboratory for assistance in carrying out the numerical computations. This work was carried out in part under the auspices of the U.S. Department of Energy by the Lawrence Livermore Laboratory under contract number W-7405-ENG-48.

REFERENCES

1. Lavoie, G. A., and Blumberg, P. N., "A Fundamental Model for Predicting Fuel Consumption, NO_x and HC Emissions of the Conventional Spark Ignited Engine", to be published in Combustion Science and Technology.
2. Lavoie, G. A., LoRusso, J. A., and Adamczyk, A. A., "Hydrocarbon Emissions Modelling for Spark Ignition Engines", paper presented at the General Motors Symposium on Combustion Modeling in Reciprocating Engines, Warren, Michigan, November 6-7, 1978.
3. Daniel, W. A., "Flame Quenching at the Walls of an Internal Combustion Engine", Sixth Symposium (International) on Combustion, Reinhold, New York,1956.
4. Wentworth, J. T., "The Piston Crevice Volume Effect on Exhaust Hydrocarbon Emissions", Combustion Science and Technology 4, 97 (1971).
5. Wentworth, J. T., "More on Origins of Exhaust Hydrocarbons- Effects of Zero Oil Consumption, Deposit Location, and Surface Roughness", SAE paper 720939, 1972.
6. Daniel, W. A., "Engine Variable Effects on Exhaust Hydrocarbon Composition (A single-cylinder engine study with propane as the fuel)", SAE paper 670124, 1967.
7. Agnew, J. T., "Unburned Hydrocarbons in Closed Vessel Explosions, Theory vs. Experiment; Applications to Spark Ignition Engine Exhaust", SAE paper 670125, 1967.
8. von Karman, T., and Millan, G., "Thermal Theory of a Laminar Flame Front near a Cold Wall", Fourth Symposium (International) on Combustion, The Combustion Institute, 1953.

9. Fendell, F. E., "Wall Quench and Flammability Limit Effects on Exhaust Hydrocarbon Emissions", Final report, Phase 2, ERDA Contract E(04-3)-1267,1977.

10. Kurkov, A. P., and Mirsky, W., "An Analysis of the Mechanism of Flame Extinction by a Cold Wall", Twelfth Symposium (International) on Combustion, The Combustion Institute, Pittsburgh, 1968.

11. Adamczyk, A. A., and Lavoie, G. A., "Laminar Head-on Flame Quenching: A Theoretical Study", SAE Transactions 87, 1978, SAE paper 780969.

12. Carrier, G. F., Fendell, F. E., Bush, W. B., and Feldman, P. S., "Nonisenthalpic Interaction of a Planar Premixed Laminar Flame with a Parallel End Wall", SAE paper 790245, 1979.

13. Lund, C. M., "HCT - A General Computer Program for Calculating Time-Dependent Phenomena Involving One-Dimensional Hydrodynamics, Transport, and Detailed Chemical Kinetics", University of California Lawrence Livermore Laboratory report UCRL-52504, 1978.

14. Westbrook, C. K., and Dryer, F. L., "Modeling of Flame Properties of Methanol", proceedings of the Alcohol Fuels Technology Third International Symposium, Asilomar, California, May, 1979.

15. Westbrook, C. K., and Dryer, F. L., "Prediction of Laminar Flame Properties of Methanol-Air Mixtures", to be published in Combustion and Flame.

16. Wentworth, J. T., "Effect of Combustion Chamber Surface Temperature on Exhaust Hydrocarbon Concentration", SAE paper 710587, 1971.

17. Westbrook, C. K., and Dryer, F. L., "A Comprehensive Mechanism for Methanol Oxidation", Combustion Science and Technology 20, 125 (1979).

18. Westbrook, C. K., "An Analytical Study of the Shock Tube Ignition of Mixtures of Methane and Ethane", Combustion Science and Technology 20, 5 (1979).

19. Westbrook, C. K., Creighton, J., Lund, C., and Dryer, F. L., "A Numerical Model of Chemical Kinetics of Combustion in a Turbulent Flow Reactor", J. Phys. Chem. 81, 2542 (1977).

20. Ferguson, C. R., and Keck, J. C., "On Laminar Flame Quenching and its Application to Spark Ignition Engines", Combustion and Flame 28, 197 (1977).

21. Ishikawa, N., and Branch, M. C., "A Simple Model of Transient Thermal Flame Quenching", SAE paper 770648, 1977.

22. Tsatsaronis, G., "Prediction of Propagating Laminar Flames in Methane, Oxygen, Nitrogen Mixtures", Combustion and Flame 33, 217 (1978).

23. Smith, O. I., Westbrook, C. K., and Sawyer, R. F., "Lean Limit Combustion in an Expanding Chamber", Seventeenth Symposium (International) on Combustion, The Combustion Institute, in press.

24. Westbrook, C. K., "Propagation of a Flame Through a Stratified Charge Combustion Chamber", Acta Astronautica 5, 1185 (1978).

25. Westbrook, C. K., "Fuel Motion and Pollutant Formation in Stratified Charge Combustion", SAE paper 790248, 1979.

26. Andrews, G. E., and Bradley, D., "The Burning Velocity of Methane-Air Mixtures", Combustion and Flame 19, 275 (1972).

27. Semenov, N. N., "Thermal Theory of Combustion and Explosion. III. Theory of Normal Flame Propagation", NASA TM 1026, 1942.

28. Lavoie, G. A., "Correlations of Combustion Data for S. I. Engine Calculations: Laminar Flame Speed, Quench Distance and Global Reaction Rates", SAE Transactions 87, 1978, paper 780229.

29. Metghalchi, M., and Keck, J. C., "Laminar Burning Velocity of Propane-Air Mixtures at High Temperature and Pressure", paper presented at the Spring Meeting of the Central States Section of the Combustion Institute, Columbus, Indiana, April 1979.

30. Bergner, P., Eberius, H., and Pokorny, H., "Flame Quenching and Exhaust Hydrocarbons in a Combustion Bomb as a Function of Pressure, Temperature, and Equivalence Ratio for Methanol and Other Alcohols", proceedings of the Alcohol Fuels Technology Third International Symposium, Asilomar, California, May 1979.

31. LoRusso, J. A., Kaiser, E. W., and Lavoie, G. A., "In-Cylinder Sampling Valve Measurement of Hydrocarbons in a Spark Ignited Engine", to be presented at the Eastern States Section of the Combustion Institute, Atlanta, November 7-9, 1979.

32. Ellenberger, J. M., and Bowlus, D. A., "Single Wall Quench Distance Measurements", paper presented at the 1971 Technical Session, Central States Section, The Combustion Institute, March, 1971.

TABLE CAPTIONS

1. Model equations, including conservation of mass, momentum, energy, and each chemical species mass fraction. Also shown are the general form of the reaction rate expressions and the equation of state.
2. Detailed chemical kinetic reaction mechanism. See reference [17] for further references on the reaction rate data.

Table I

Model equations

$$\frac{\partial \rho}{\partial t} + \frac{\partial \rho u}{\partial x} = 0$$

$$\frac{\partial \rho u}{\partial t} + \frac{\partial \rho u^2}{\partial x} = - \frac{\partial (P + Q)}{\partial x}$$

$$\frac{\partial \rho}{\partial t} + \frac{\partial \rho u h_s}{\partial x} = \frac{\partial}{\partial x} \left(\rho C_p \alpha \frac{\partial T}{\partial x} \right) + \frac{\partial}{\partial x} \left(\rho \sum h_i D_i \frac{\partial y_i}{\partial x} \right) + \rho \dot{q} + S_w$$

$$\frac{\partial \rho y_i}{\partial t} + \frac{\partial \rho u y_i}{\partial x} = \frac{\partial}{\partial x} \left(\rho D_i \frac{\partial y_i}{\partial x} \right) + (\rho \dot{y}_i)_{k \text{ in}}$$

$$K = A T^n e^{-E_{a/RT}}$$

$$P = RT \sum c_i$$

Table II

Methanol oxidation mechanism. Reaction rates in cm^3-mole-sec-kcal units, $k = AT^n \exp(-E_a/RT)$

	Reaction		Rate		
			log A	n	E_a
1	$CH_3OH + M$	$\rightarrow CH_3 + OH + M$	18.5	0	80.0
2	$CH_3OH + O_2$	$\rightarrow CH_2OH + HO_2$	13.6	0	50.9
3	$CH_3OH + OH$	$\rightarrow CH_2OH + H_2O$	12.6	0	2.0
4	$CH_3OH + O$	$\rightarrow CH_2OH + OH$	12.2	0	2.3
5	$CH_3OH + H$	$\rightarrow CH_2OH + H_2$	13.5	0	7.0
6	$CH_3OH + H$	$\rightarrow CH_3 + H_2O$	12.7	0	5.3
7	$CH_3OH + CH_3$	$\rightarrow CH_2OH + CH_4$	11.3	0	9.8
8	$CH_3OH + HO_2$	$\rightarrow CH_2OH + H_2O_2$	12.8	0	19.4
9	$CH_2OH + M$	$\rightarrow CH_2O + H + M$	13.4	0	29.0
10	$CH_2OH + O_2$	$\rightarrow CH_2O + HO_2$	12.0	0	6.0
11	$CH_4 + M$	$\rightarrow CH_3 + H + M$	17.1	0	88.4
12	$CH_4 + H$	$\rightarrow CH_3 + H_2$	14.1	0	11.9
13	$CH_4 + OH$	$\rightarrow CH_3 + H_2O$	3.5	3.08	2.0
14	$CH_4 + O$	$\rightarrow CH_3 + OH$	13.2	0	9.2
15	$CH_4 + HO_2$	$\rightarrow CH_3 + H_2O_2$	13.3	0	18.0
16	$CH_3 + HO_2$	$\rightarrow CH_3O + OH$	13.2	0	0.0
17	$CH_3 + OH$	$\rightarrow CH_2O + H_2$	12.6	0	0.0
18	$CH_3 + O$	$\rightarrow CH_2O + H$	14.1	0	2.0
19	$CH_3 + O_2$	$\rightarrow CH_3O + O$	13.4	0	29.0
20	$CH_2O + CH_3$	$\rightarrow CH_4 + HCO$	10.0	0.5	6.0
21	$CH_3 + HCO$	$\rightarrow CH_4 + CO$	11.5	0.5	0.0
22	$CH_3 + HO_2$	$\rightarrow CH_4 + O_2$	12.0	0	0.4
23	$CH_3O + M$	$\rightarrow CH_2O + H + M$	13.7	0	21.0
24	$CH_3O + O_2$	$\rightarrow CH_2O + HO_2$	12.0	0	6.0
25	$CH_2O + M$	$\rightarrow HCO + H + M$	16.7	0	72.0

Table II (Continued)

Methanol oxidation mechanism. Reaction rates in cm^3-mole-sec-kcal units, $k = AT^n \exp(-E_a/RT)$

	Reaction		Rate		
			log A	n	E_a
26	$CH_2O + OH$	$\rightarrow HCO + H_2O$	14.7	0	6.3
27	$CH_2O + H$	$\rightarrow HCO + H_2$	12.6	0	3.8
28	$CH_2O + O$	$\rightarrow HCO + OH$	13.7	0	4.6
29	$CH_2O + HO_2$	$\rightarrow HCO + H_2O_2$	12.0	0	8.0
30	$HCO + OH$	$\rightarrow CO + H_2O$	14.0	0	0.0
31	$HCO + M$	$\rightarrow H + CO + M$	14.2	0	19.0
32	$HCO + H$	$\rightarrow CO + H_2$	14.3	0	0.0
33	$HCO + O$	$\rightarrow CO + OH$	14.0	0	0.0
34	$HCO + HO_2$	$\rightarrow CH_2O + O_2$	14.0	0	3.0
35	$HCO + O_2$	$\rightarrow CO + HO_2$	12.5	0	7.0
36	$CO + OH$	$\rightarrow CO_2 + H$	7.1	1.3	−0.8
37	$CO + HO_2$	$\rightarrow CO_2 + OH$	14.0	0	23.0
38	$CO + O + M$	$\rightarrow CO_2 + M$	15.8	0	4.1
39	$CO_2 + O$	$\rightarrow CO + O_2$	12.4	0	43.8
40	$H + O_2$	$\rightarrow O + OH$	14.3	0	16.8
41	$H_2 + O$	$\rightarrow H + OH$	10.3	1	8.9
42	$H_2O + O$	$\rightarrow OH + OH$	13.5	0	18.4
43	$H_2O + H$	$\rightarrow H_2 + OH$	14.0	0	20.3
44	$H_2O_2 + OH$	$\rightarrow H_2O + HO_2$	13.0	0	1.8
45	$H_2O + M$	$\rightarrow H + OH + M$	16.3	0	105.1
46	$H + O_2 + M$	$\rightarrow HO_2 + M$	15.2	0	−1.0
47	$HO_2 + O$	$\rightarrow OH + O_2$	13.7	0	1.0
48	$HO_2 + H$	$\rightarrow OH + OH$	14.4	0	1.9
49	$HO_2 + H$	$\rightarrow H_2 + O_2$	13.4	0	0.7

Table II (Continued)

Methanol oxidation mechanism. Reaction rates in cm^3-mole-sec-kcal units, $k = AT^n \exp(-E_a/RT)$

	Reaction		Rate		
			log A	n	E_a
50	$HO_2 + OH$	$\rightarrow H_2O + O_2$	13.7	0	1.0
51	$H_2O_2 + O_2$	$\rightarrow HO_2 + HO_2$	13.6	0	42.6
52	$H_2O_2 + M$	$\rightarrow OH + OH + M$	17.1	0	45.5
53	$H_2O_2 + H$	$\rightarrow HO_2 + H_2$	12.2	0	3.8
54	$O + H + M$	$\rightarrow OH + M$	16.0	0	0.0
55	$O_2 + M$	$\rightarrow O + O + M$	15.7	0	115.0
56	$H_2 + M$	$\rightarrow H + H + M$	14.3	0	96.0
57	C_2H_6	$\rightarrow CH_3 + CH_3$	19.4	−1	88.3
58	$C_2H_6 + CH_3$	$\rightarrow C_2H_5 + CH_4$	−0.3	4	8.3
59	$C_2H_6 + H$	$\rightarrow C_2H_5 + H_2$	2.7	3.5	5.2
60	$C_2H_6 + OH$	$\rightarrow C_2H_5 + H_2O$	13.8	0	2.4
61	$C_2H_6 + O$	$\rightarrow C_2H_5 + OH$	13.4	0	6.4
62	C_2H_5	$\rightarrow C_2H_4 + H$	13.6	0	38.0
63	$C_2H_5 + O_2$	$\rightarrow C_2H_4 + HO_2$	12.0	0	5.0
64	$C_2H_5 + C_2H_3$	$\rightarrow C_2H_4 + C_2H_4$	17.5	0	35.6
65	$C_2H_4 + O$	$\rightarrow CH_3 + HCO$	13.0	0	1.1
66	$C_2H_4 + M$	$\rightarrow C_2H_3 + H + M$	17.6	0	98.2
67	$C_2H_4 + H$	$\rightarrow C_2H_3 + H_2$	13.8	0	6.0
68	$C_2H_4 + OH$	$\rightarrow C_2H_3 + H_2O$	14.0	0	3.5
69	$C_2H_4 + O$	$\rightarrow CH_2O + CH_2$	13.4	0	5.0
70	$C_2H_3 + M$	$\rightarrow C_2H_2 + H + M$	16.5	0	40.5
71	$C_2H_2 + M$	$\rightarrow C_2H + H + M$	14.0	0	114.0
72	$C_2H_2 + O_2$	$\rightarrow HCO + HCO$	12.6	0	28.0
73	$C_2H_2 + H$	$\rightarrow C_2H + H_2$	14.3	0	19.0
74	$C_2H_2 + OH$	$\rightarrow C_2H + H_2O$	12.8	0	7.0

Table II (Continued)

Methanol oxidation mechanism. Reaction rates in cm^3-mole-sec-kcal units, $k = AT^n \exp(-E_a/RT)$

	Reaction		Rate		
			log A	n	E_a
75	$C_2H_2 + O$	$\rightarrow C_2H + OH$	15.5	−0.6	17.0
76	$C_2H_2 + O$	$\rightarrow CH_2 + CO$	13.8	0	4.0
77	$C_2H + O_2$	$\rightarrow HCO + CO$	13.0	0	7.0
78	$C_2H + O$	$\rightarrow CO + CH$	13.7	0	0.0
79	$CH_2 + O_2$	$\rightarrow HCO + OH$	14.0	0	3.7
80	$CH_2 + O$	$\rightarrow CH + OH$	11.3	0.68	25.0
81	$CH_2 + H$	$\rightarrow CH + H_2$	11.4	0.67	25.7
82	$CH_2 + OH$	$\rightarrow CH + H_2O$	11.4	0.67	25.7
83	$CH + O_2$	$\rightarrow CO + OH$	11.1	0.67	25.7
84	$CH + O_2$	$\rightarrow HCO + O$	13.0	0	0.0

FIGURE CAPTIONS

1. Schematic view of head-on flame quenching. The graphical definitions of the thermal flame thickness L_t and flame positions q_t and q_r are also indicated.
2. Temperature and species concentration profiles for unquenched methanol-air flame. (a) Temperature and major species;(b) Major radical and intermediate species; (c) Minor species.
3. Temperature and species concentration profiles at time of quenching for reference methanol-air case. (a) Temperature and major species; (b) Major radical and intermediate species; (c) Minor intermediate species.
4. Unburned fuel concentration profiles at three indicated times following quench time, for reference methanol-air case.
5. Average fuel concentration and flame position, both as functions of time relative to quench time t_q, for the methanol-air reference case.
6. Average fuel concentration for the methane-air and methanol-air reference cases, showing the effect of fuel type.
7. Quench distance as a function of equivalence ratio, for methane-air and methanol-air fuels.
8. Average fuel concentration as a function of time relative to quench time t_q, showing the effects of equivalence ratio. (a) Methanol-air (b) Methane-air
9. Variation of quench distance with pressure, for both fuels studied.
10. Average fuel concentration as function of time relative to quench time t_q, showing the effects of pressure. (a) Methanol-air (b) Methane-air

11. Average fuel concentrations as functions of pressure. The curves which are keyed to the scale at the left refer to fuel concentrations at quench time t_q, and the curves keyed to the scale at the right refer to levels one millisecond after quench time. Solid curves are for methane, dashed curves for methanol.

12. Average fuel concentrations as functions of time relative to quench time t_q, showing the effects of wall temperature T_w. Results shown are for methanol-air at 10 atm pressure.

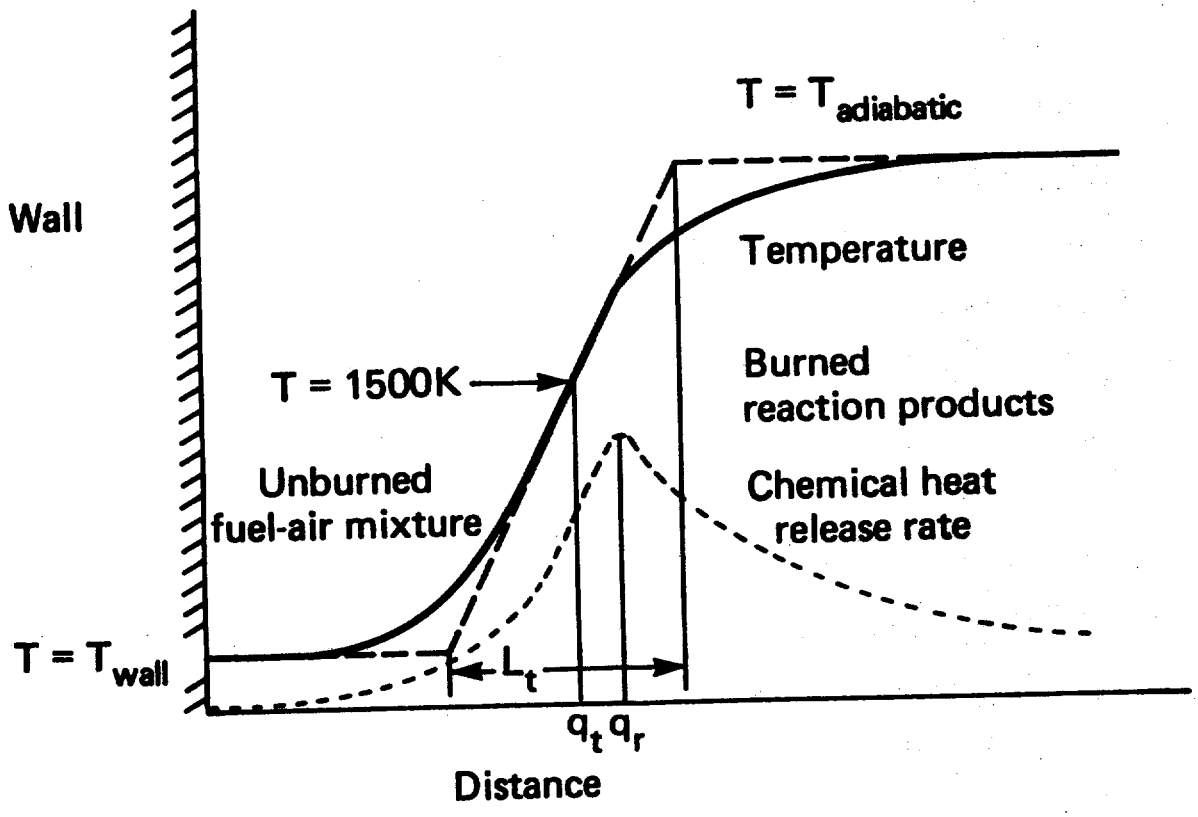
Wall
T = T adiabatic
Temperature
T = 1500K
Burned
reaction products
Unburned
fuel-air mixture
Chemical heat
release rate
T = T wall
L t
q t q r
Distance

Figure 1

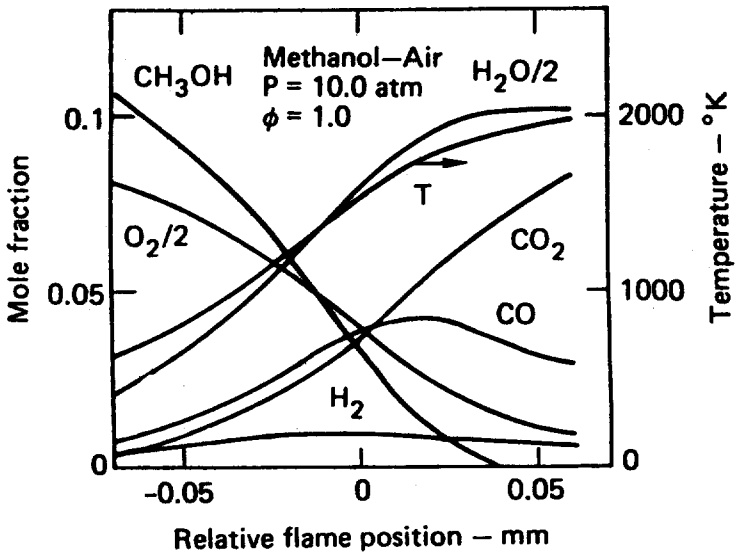
Methanol—Air
P = 10.0 atm
ϕ = 1.0
CH_3OH
$H_2O/2$
T
$O_2/2$
CO_2
CO
H_2
0.1
0.05
0
2000
1000
0
-0.05
0
0.05
Mole fraction
Temperature — °K
Relative flame position — mm

Figure 2a

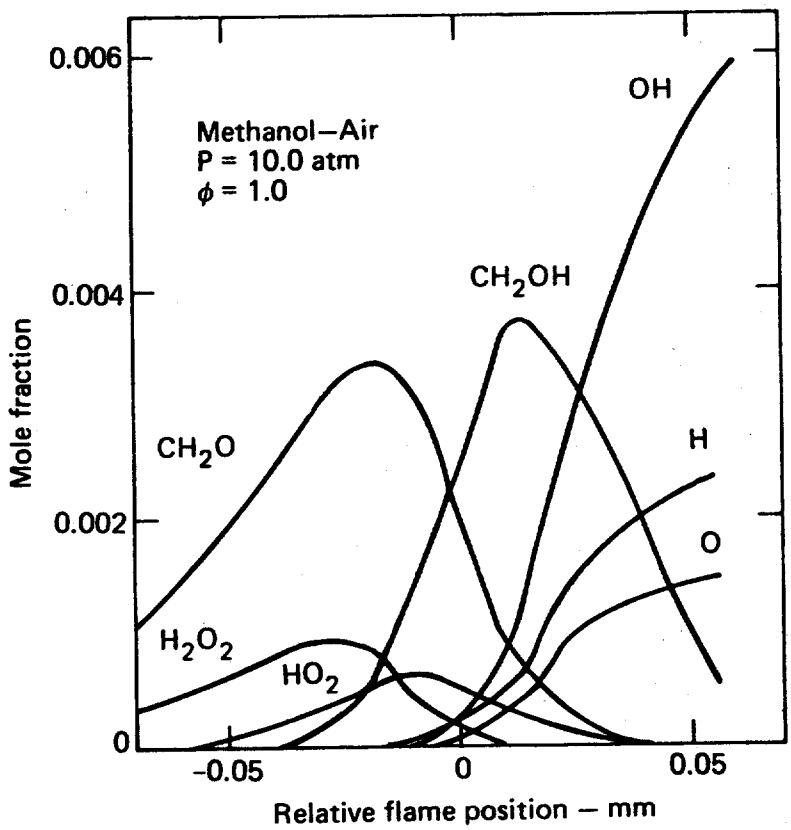
0.006
0.004
0.002
0
Mole fraction
Methanol—Air
P = 10.0 atm
ϕ = 1.0
OH
CH_2OH
CH_2O
H
O
H_2O_2
HO_2
-0.05
0
0.05
Relative flame position — mm

Figure 2b

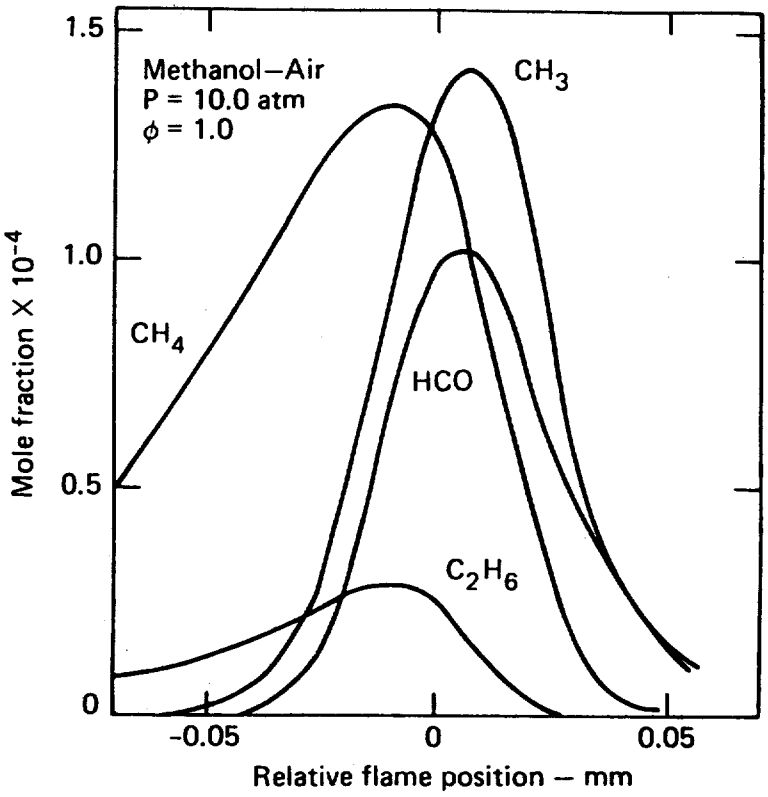
1.5
1.0
0.5
0
Methanol—Air
P = 10.0 atm
ϕ = 1.0
CH_3
CH_4
HCO
C_2H_6
Mole fraction X 10^{-4}
-0.05
0
0.05
Relative flame position — mm

Figure 2c

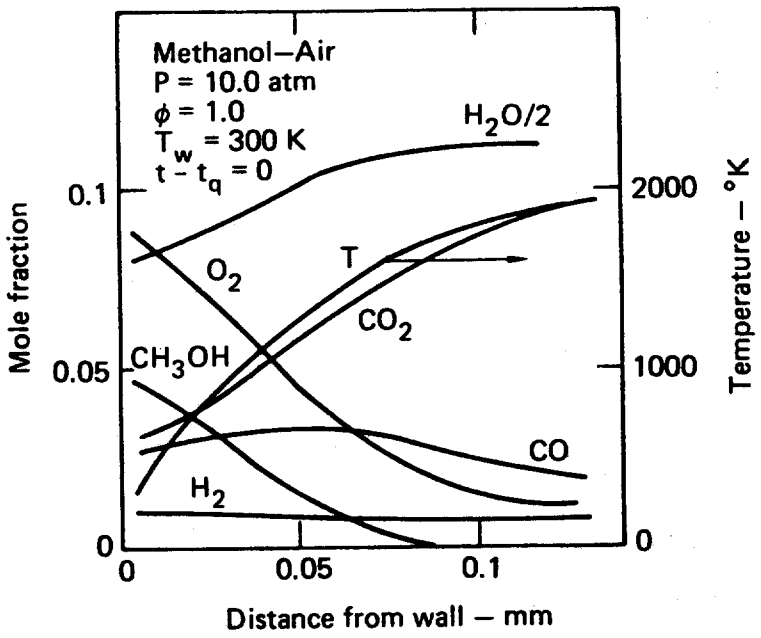
Methanol–Air
P = 10.0 atm
ϕ = 1.0
T_w = 300 K
$t - t_q$ = 0
$H_2O/2$
O_2
T
CO_2
CH_3OH
CO
H_2
0.1
0.05
0
2000
1000
0
0
0.05
0.1
Mole fraction
Temperature – °K
Distance from wall – mm

Figure 3a

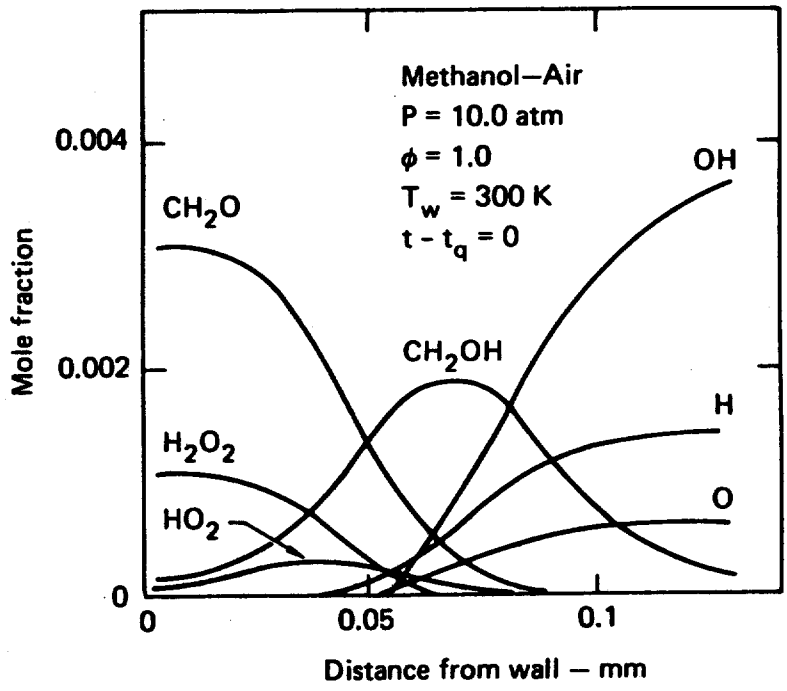
Methanol—Air
P = 10.0 atm
ϕ = 1.0
T_w = 300 K
$t - t_q = 0$
CH_2O
OH
CH_2OH
H
H_2O_2
O
HO_2
0.004
0.002
0
0
0.05
0.1
Mole fraction
Distance from wall — mm

Figure 3b

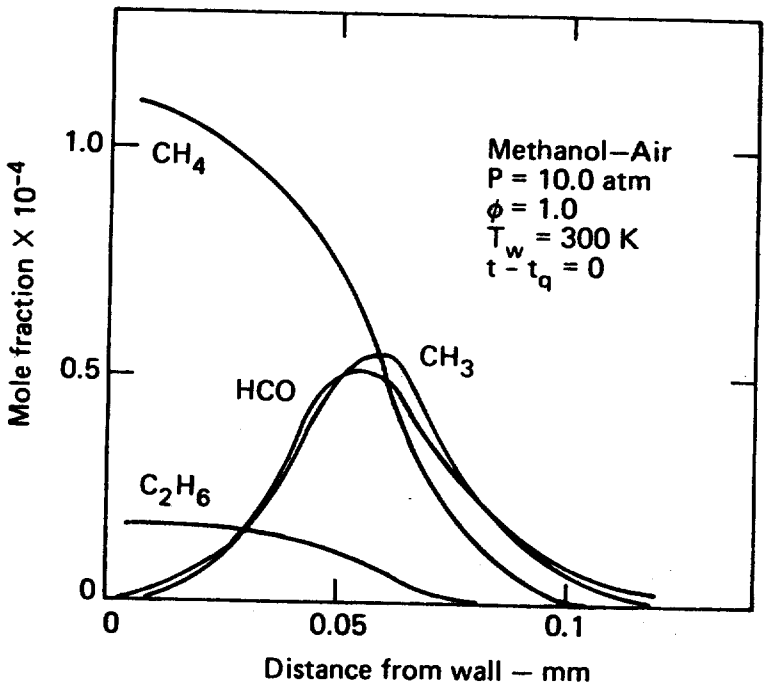
Methanol–Air
P = 10.0 atm
ϕ = 1.0
T_w = 300 K
$t - t_q$ = 0
CH_4
CH_3
HCO
C_2H_6
1.0
0.5
0
0
0.05
0.1
Mole fraction X 10^{-4}
Distance from wall — mm

Figure 3c

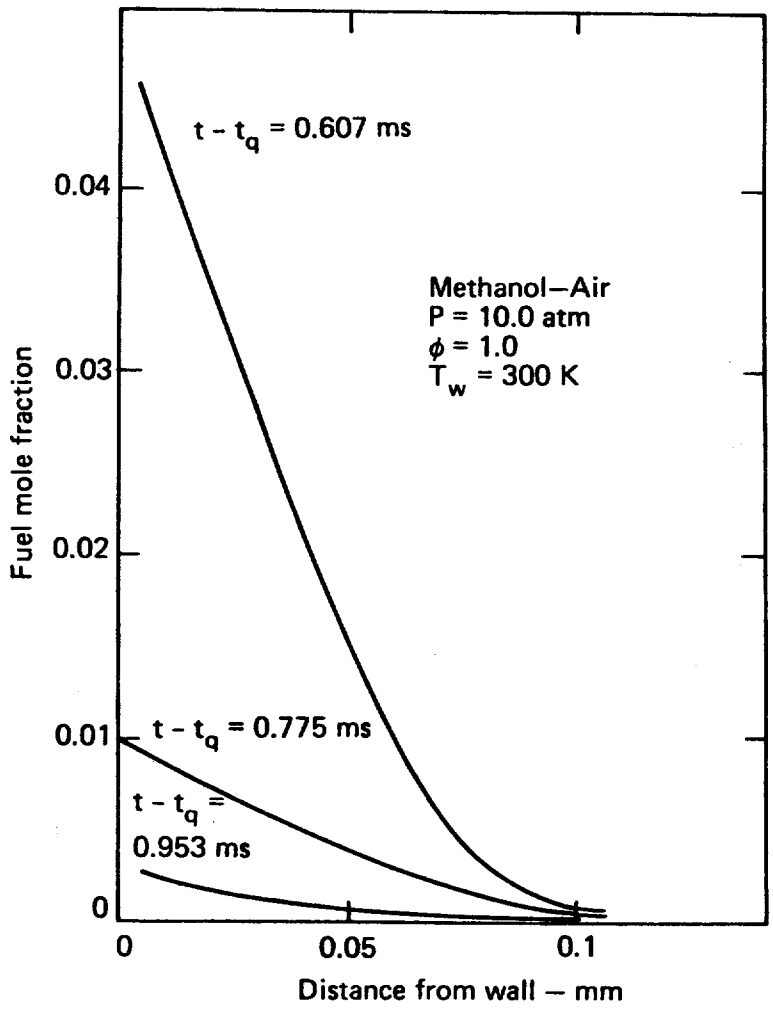
t - t_q = 0.607 ms
Methanol–Air
P = 10.0 atm
ϕ = 1.0
T_w = 300 K
t - t_q = 0.775 ms
t - t_q =
0.953 ms
Fuel mole fraction
0.04
0.03
0.02
0.01
0
0
0.05
0.1
Distance from wall — mm

Figure 4

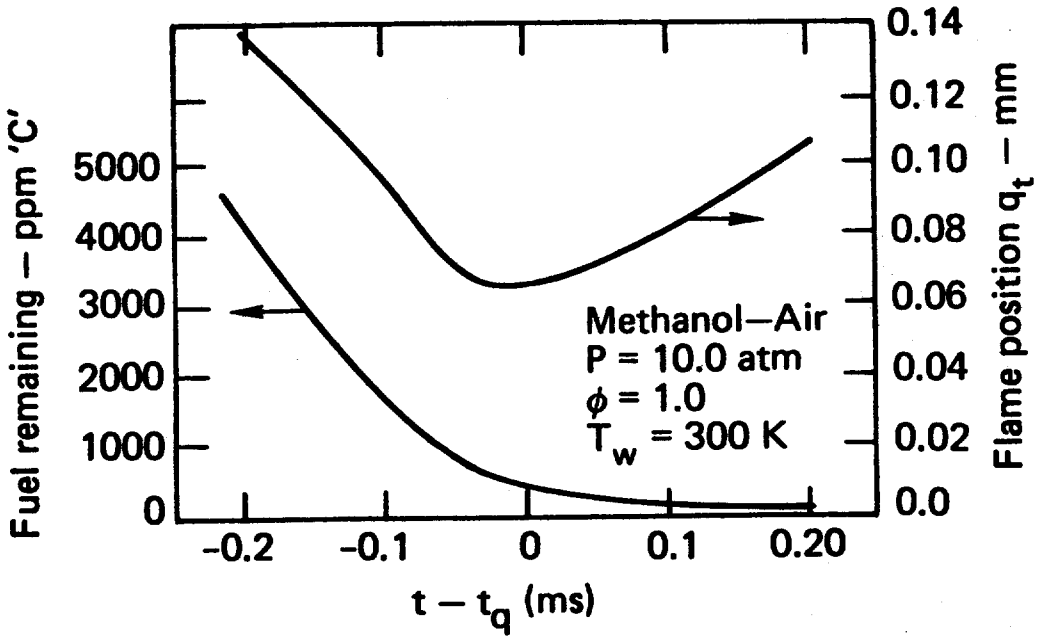
Fuel remaining – ppm 'C'
5000
4000
3000
2000
1000
0
-0.2
-0.1
0
0.1
0.20
t – t_q (ms)
0.14
0.12
0.10
0.08
0.06
0.04
0.02
0.0
Flame position q_t – mm
Methanol–Air
P = 10.0 atm
ϕ = 1.0
T_w = 300 K

Figure 5

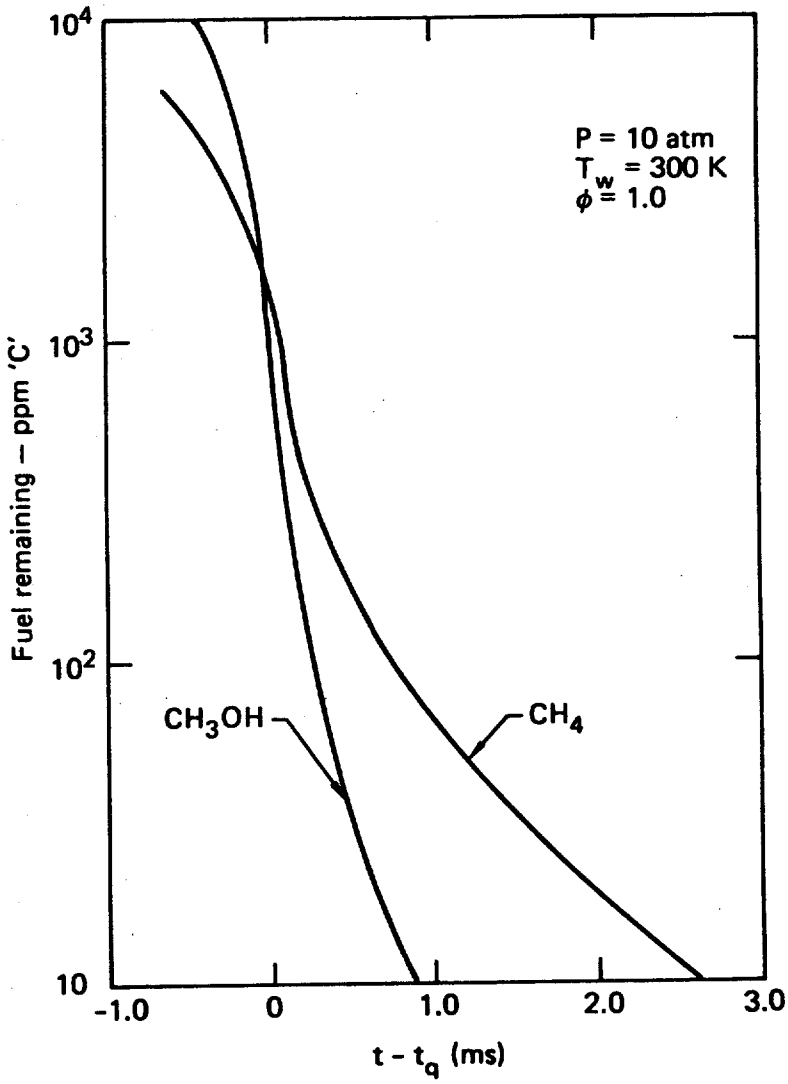
10^4
10^3
10^2
10
Fuel remaining – ppm 'C'
P = 10 atm
T_w = 300 K
ϕ = 1.0
CH_3OH
CH_4
-1.0
0
1.0
2.0
3.0
t - t_q (ms)

Figure 6

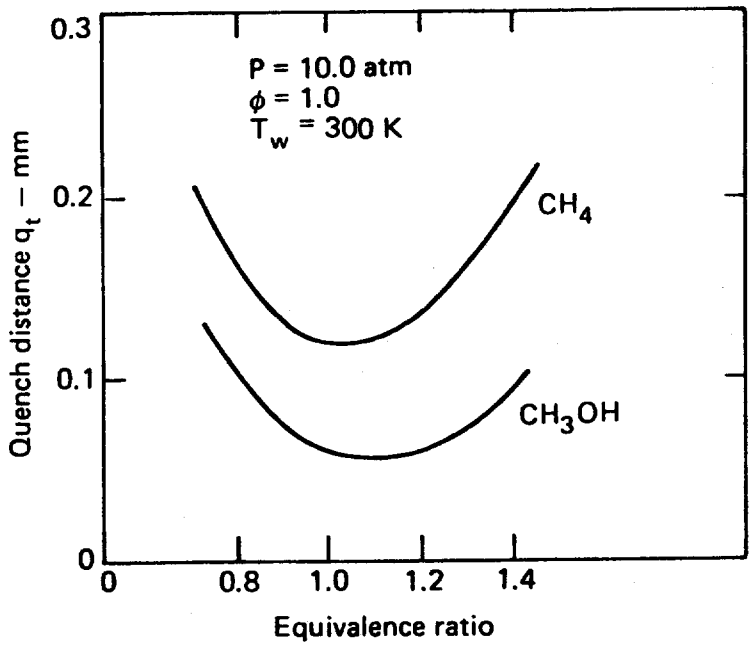
0.3
0.2
0.1
0
P = 10.0 atm
ϕ = 1.0
T_w = 300 K
CH_4
CH_3OH
Quench distance q_t – mm
0
0.8
1.0
1.2
1.4
Equivalence ratio

Figure 7

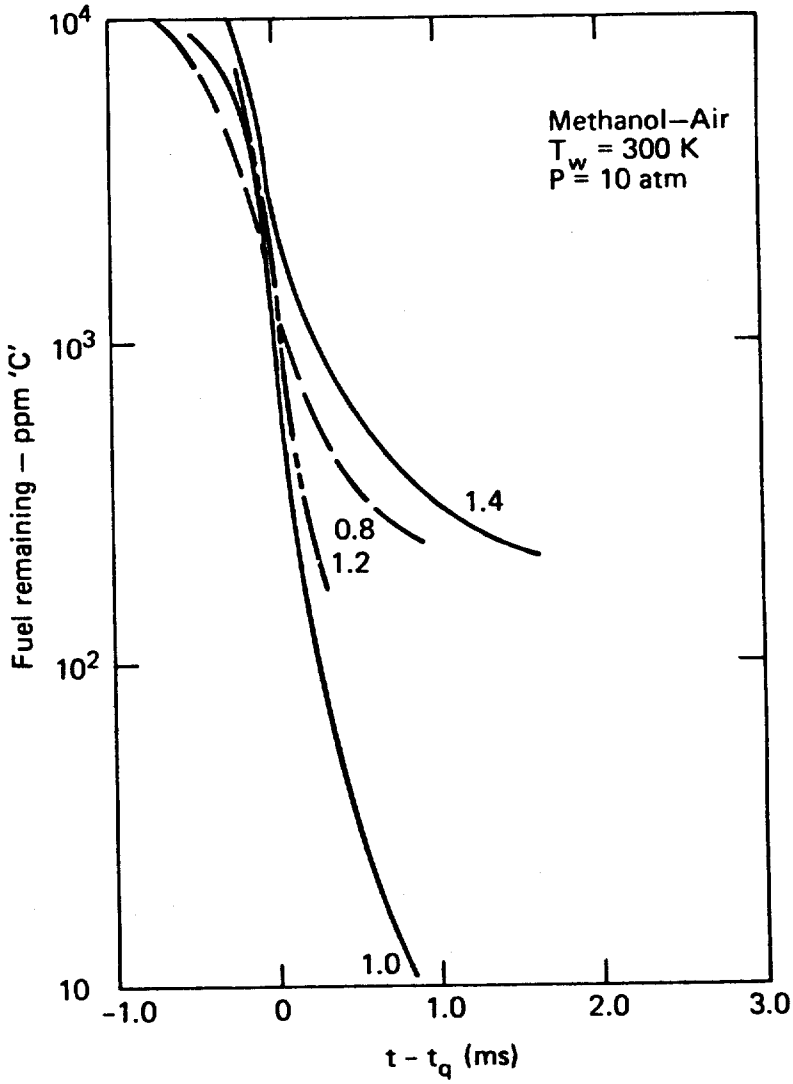
Methanol–Air
T_w = 300 K
P = 10 atm
1.4
0.8
1.2
1.0
10^4
10^3
10^2
10
Fuel remaining – ppm 'C'
-1.0
0
1.0
2.0
3.0
t - t_q (ms)

Figure 8a

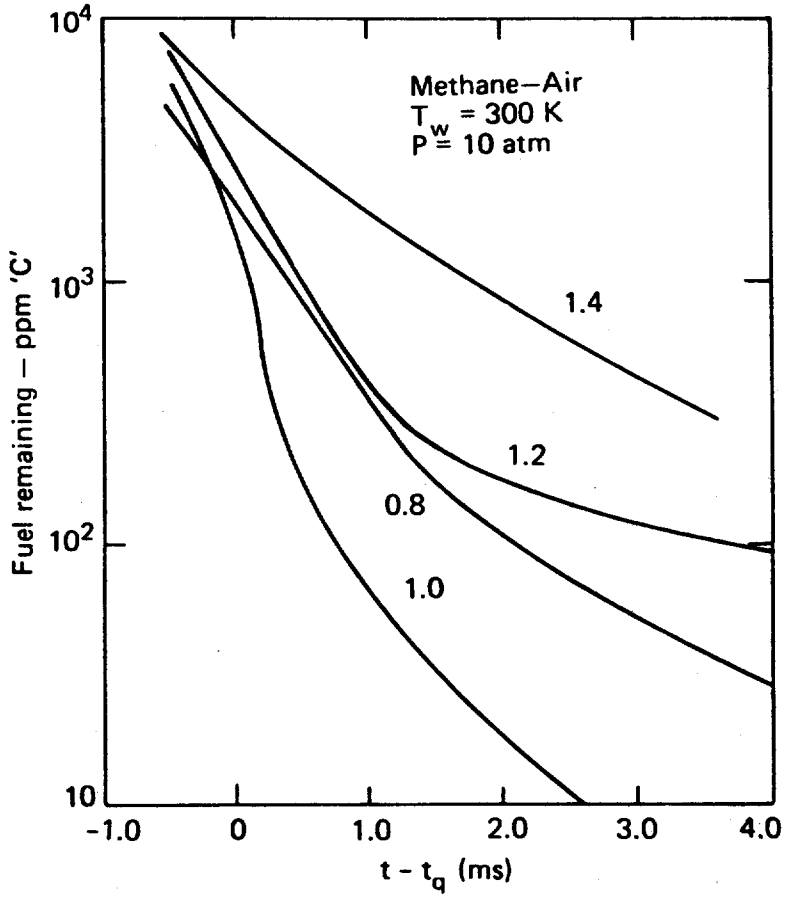
Methane–Air
T_w = 300 K
P = 10 atm
1.4
1.2
0.8
1.0
10^4
10^3
10^2
10
Fuel remaining – ppm 'C'
-1.0
0
1.0
2.0
3.0
4.0
t - t_q (ms)

Figure 8b

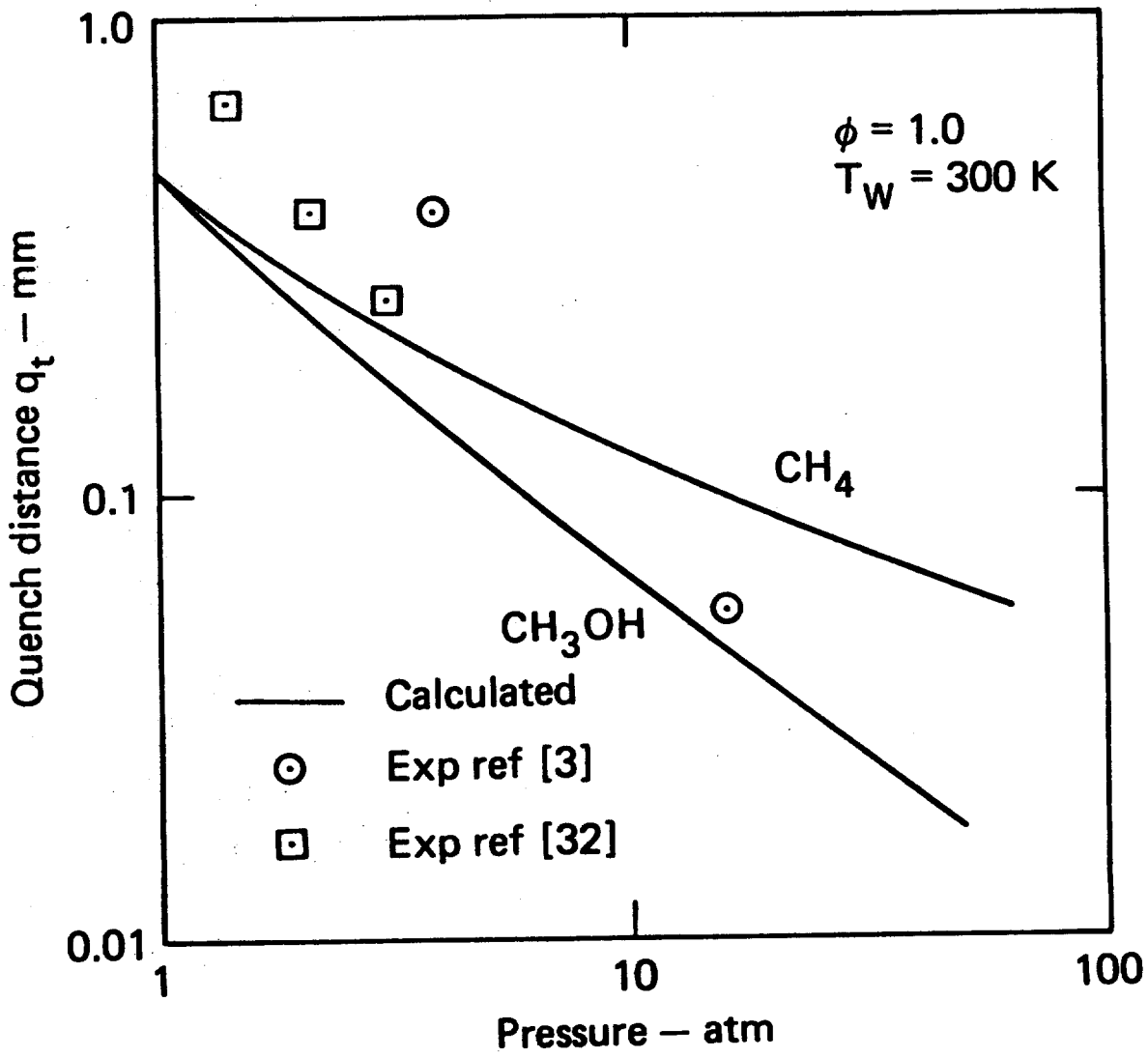
1.0
0.1
0.01
1
10
100
Quench distance q_t — mm
Pressure — atm
ϕ = 1.0
T_W = 300 K
CH_4
CH_3OH
Calculated
Exp ref [3]
Exp ref [32]

Figure 9

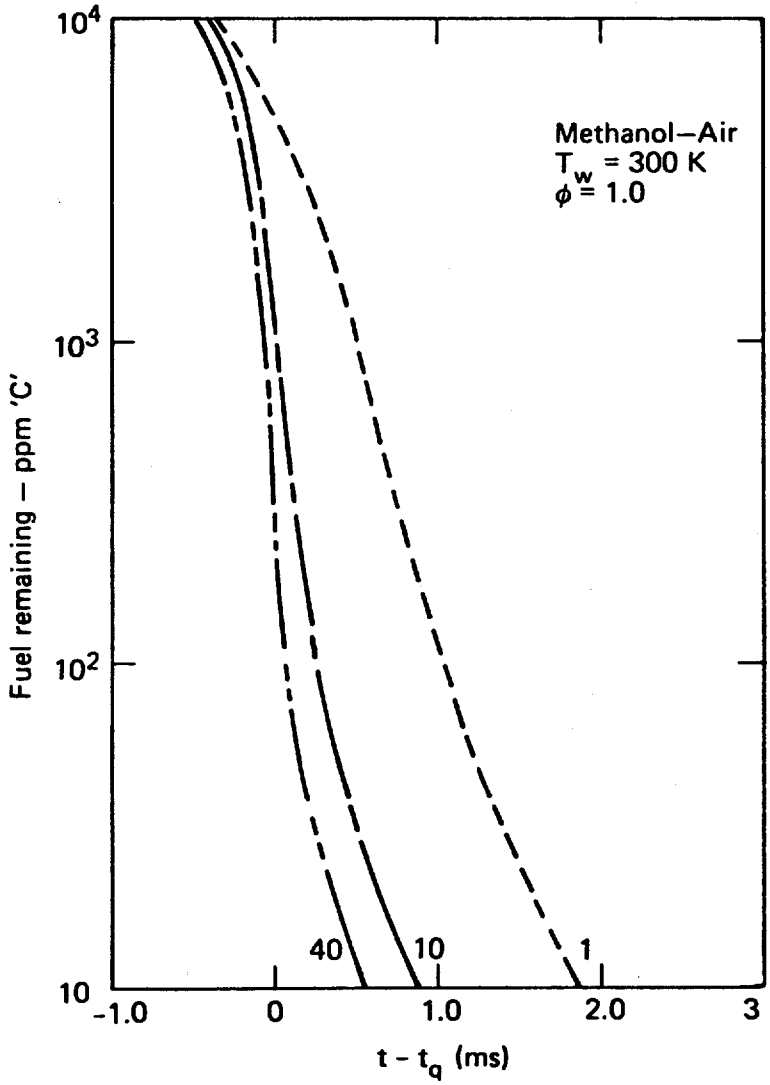
Methanol–Air
T_w = 300 K
ϕ = 1.0
Fuel remaining – ppm 'C'
10^4
10^3
10^2
10
40
10
1
-1.0
0
1.0
2.0
3
t - t_q (ms)

Figure 10a

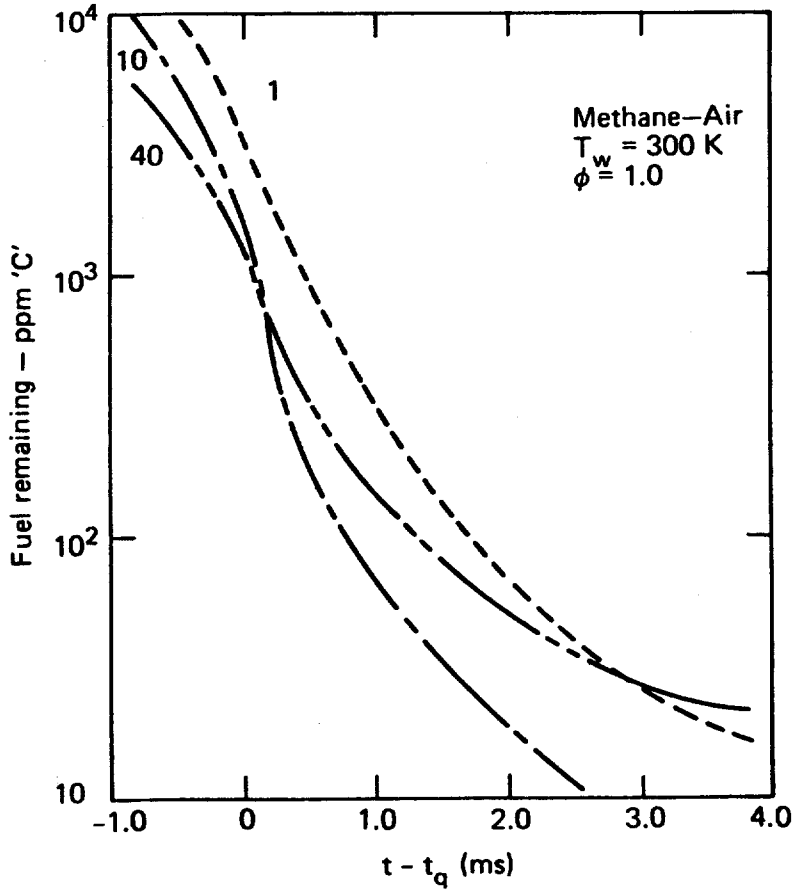
10^4
10^3
10^2
10
10
1
40
Methane–Air
T_w = 300 K
ϕ = 1.0
Fuel remaining – ppm 'C'
-1.0
0
1.0
2.0
3.0
4.0
t - t_q (ms)

Figure 10b

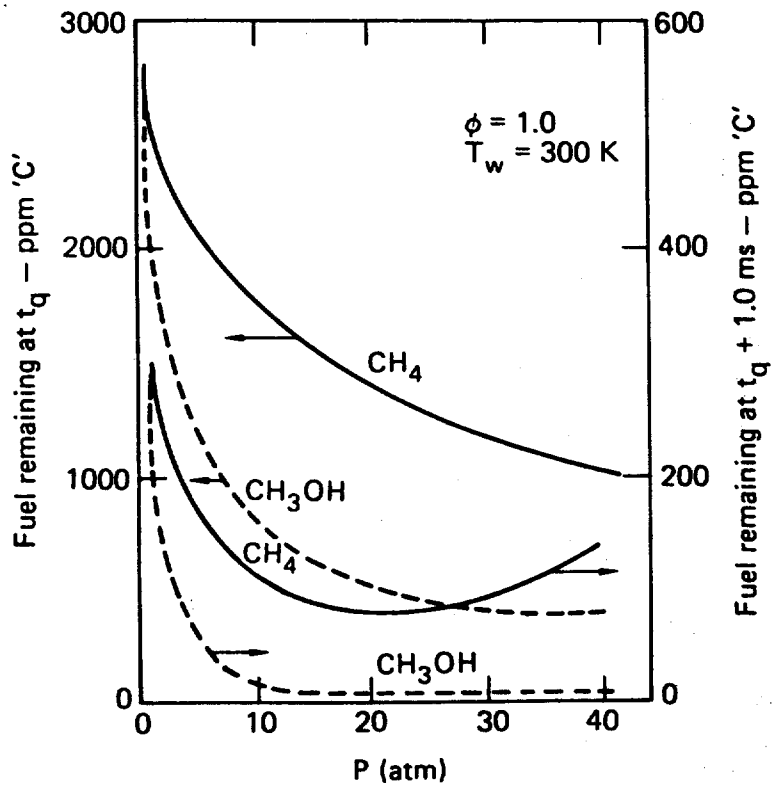
3000
2000
1000
0
600
400
200
0
0
10
20
30
40
P (atm)
ϕ = 1.0
T_w = 300 K
CH_4
CH_3OH
CH_4
CH_3OH
Fuel remaining at t_q – ppm 'C'
Fuel remaining at t_q + 1.0 ms – ppm 'C'

Figure 11

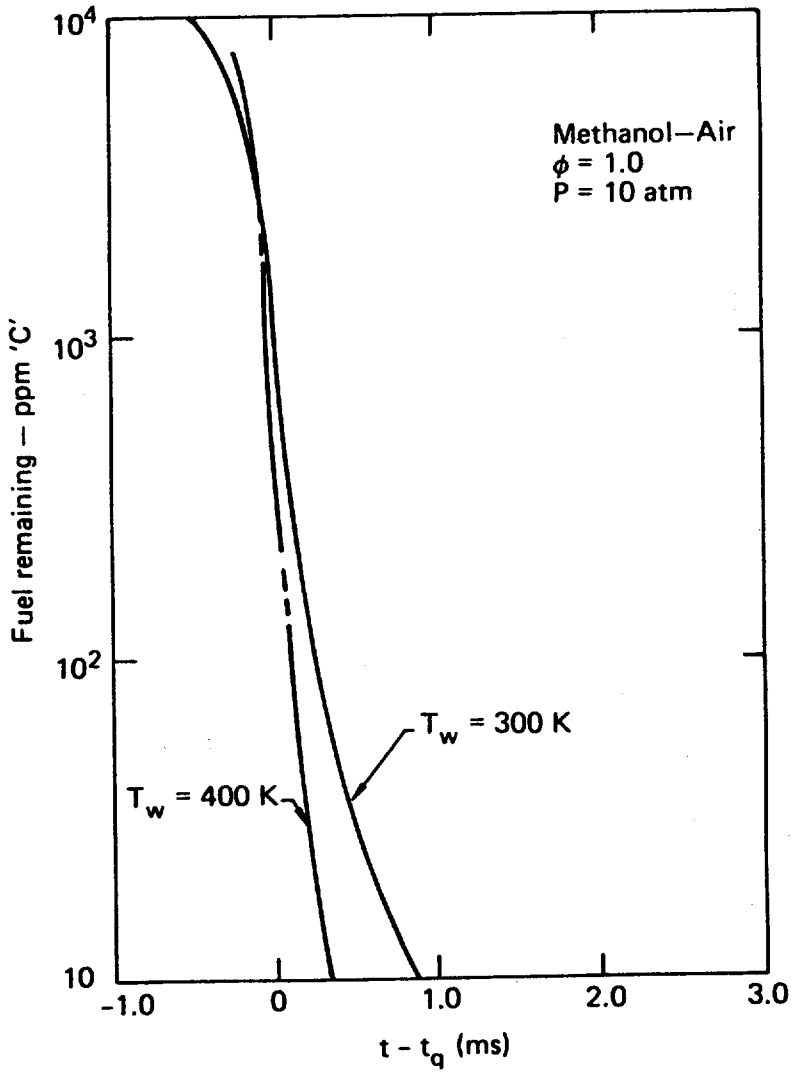
Methanol–Air
ϕ = 1.0
P = 10 atm
T_w = 300 K
T_w = 400 K
Fuel remaining – ppm 'C'
10^4
10^3
10^2
10
-1.0
0
1.0
2.0
3.0
t - t_q (ms)

Figure 12